

## **ELECTRICAL TRANSPORT PROPERTIES OF $\text{La}_{0.67}(\text{Sr}_{1-x}\text{Ba}_x)_{0.33}\text{Mn}_{0.9}\text{Ti}_{0.1}\text{O}_3$ PEROVSKITE MANGANITE**

Z.Zalita<sup>1,2</sup>, S.A.Halim<sup>1</sup>, K.P.Lim<sup>1</sup>, Z.A. Talib<sup>1</sup>, Z. Hishamuddin<sup>1</sup> and C.P. Walter<sup>1</sup>

<sup>1</sup>*Department of Physics, Faculty of Science,  
Universiti Putra Malaysia, 43400 UPM Serdang, Selangor, Malaysia*

<sup>2</sup>*School of Applied Physics, Faculty of Science and Technology,  
Universiti Kebangsaan Malaysia, 43600 UKM Bangi, Selangor, Malaysia*

### **ABSTRACT**

Influence of Ba doping on the structure and electrical transport properties of polycrystalline  $\text{La}_{0.67}(\text{Sr}_{1-x}\text{Ba}_x)_{0.33}\text{Mn}_{0.9}\text{Ti}_{0.1}\text{O}_3$  ( $0 \leq x \leq 1.00$ ) perovskite manganites were studied. The samples synthesized by solid-state reaction method experience a transformation from  $R\text{-}3C$  rhombohedral to  $Pm3m$  cubic structure with the increment of Ba concentration. Temperature dependent resistivity showed that the metal-insulator transition temperature decreases from 117 K to 60 K with increasing Ba content up to  $x = 0.75$ . The low temperature resistivity below the metal-insulator transition temperature,  $T_p$  was well fitted with the  $\rho = \rho_o + \rho_2 T^2$  equation indicating the contribution of domain or grain boundary mechanisms and the electron-electron scattering mechanism in the conduction. Contrary to that, in the high temperature insulating regime ( $T > T_p$ ), the resistivity follows variable range hopping (VRH) and small polaron hopping (SPH) conduction mechanisms.

### **INTRODUCTION**

Perovskite manganite system  $\text{Ln}_{1-x}\text{A}_x\text{MnO}_3$  where Ln is an element from the lanthanide group such as La, Nd, Pr, Y and  $\text{A} = \text{Ca}, \text{Sr}, \text{Ba}, \text{Pb}$  with a  $\text{Mn}^{3+}/\text{Mn}^{4+}$  mixed valence has stimulated an increasing interest due to their excellent magnetic and electronic properties, including the colossal magnetoresistance (CMR) effect [1] and the electrical transport properties [2]. All of these properties are strongly controlled by Mn valence states,  $\text{Mn}^{3+}$  and  $\text{Mn}^{4+}$  content ratio, electronic configuration and lattice distortion due to the different types and sizes of the ionic compounds. Generally CMR refers to a great change of electrical resistivity near the metal-insulator transition temperature when magnetic field is applied. This effect can be quantitatively explained by the double exchange (DE) mechanism where the  $e_g^1$  electrons hop from the  $\text{Mn}^{3+} (t_{2g}^3 e_g^1)$  to  $\text{Mn}^{4+} (t_{2g}^3 e_g^0)$  ion via  $\text{O}^{2-}$  ion [3]. However, the Jahn-Teller splitting of the  $\text{Mn}^{3+}$  ions is also important due to the arising of polaron effect which may contribute to the very large resistivity [4]. Several theories were also proposed for the understanding of the conduction mechanism occurring in this type of material. We have studied the structure, magnetoresistance and magnetism of  $\text{La}_{0.67}(\text{Sr}_{1-x}\text{Ba}_x)_{0.33}\text{MnO}_3$  [5]. As a continuation of our research we studied the electrical transport properties of

$\text{La}_{0.67}(\text{Sr}_{1-x}\text{Ba}_x)_{0.33}\text{Mn}_{0.9}\text{Ti}_{0.1}\text{O}_3$  with 10 % of the non-magnetic Ti substitution. Ti is used as a substitute ion due to its good solubility hence it will not effect the chemical stability of the original system [6].

## METHODOLOGY

Polycrystalline samples of perovskite  $\text{La}_{0.67}(\text{Sr}_{1-x}\text{Ba}_x)_{0.33}\text{Mn}_{0.9}\text{Ti}_{0.1}$  with 10% Ti at Mn site, with different compositions of  $x = 0.00, 0.25, 0.50, 0.75, 1.00$  were synthesized by the conventional solid-state reaction method. Appropriate proportions of high purity  $\text{La}_2\text{O}_3$ ,  $\text{SrCO}_3$ ,  $\text{BaCO}_3$ ,  $\text{MnO}_2$  and  $\text{TiO}_2$  powder were ball milled in acetone medium for a few hours. The thoroughly mixed slurry was then dried and ground before calcination at  $900^\circ\text{C}$  for 12 h to decompose the carbonates. The resultant powder was then ground and pressed into pellets and sintered at  $1350^\circ\text{C}$  for 24 h in air. The phase and structure analysis of the final products were studied using a Philips 7602 EA Almelo x-ray diffractometer (XRD) with  $\text{CuK}_\alpha$  radiation ( $\lambda = 1.5406 \text{ \AA}$ ) in a wide range of Bragg's angles  $2\theta$  ( $20^\circ \leq \theta \leq 80^\circ$ ) and a scanning rate of  $4^\circ/\text{min}$ . The dc resistivity measurement was carried out using the standard four-point probe method from 40 K to 275 K in the absence of magnetic field.

## RESULTS AND DISCUSSION

Figure 1 shows the XRD spectra of all the prepared samples which were found to be of single phase perovskite without any detectable secondary phases or impurity which confirms the completion of the solid state reaction and the incorporation of Ba and Ti into the Sr and Mn sites. XRD patterns for samples with  $x = 0.00$  and  $0.25$  could be indexed to a distorted rhombohedral crystal structures with  $R\bar{3}c$  space group, with  $a = 5.5141 \text{ \AA}$ ,  $c = 13.3715 \text{ \AA}$  and  $a = 5.4997 \text{ \AA}$ ,  $c = 13.5336 \text{ \AA}$  respectively. All the prominent peaks shift to lower angle when Ba concentration increases due to the larger ionic radius of  $\text{Ba}^{2+}$  ( $1.35 \text{ \AA}$ ) than  $\text{Sr}^{2+}$  ( $1.18 \text{ \AA}$ ) [5]. At higher Ba concentration ( $x = 0.75$  and  $1.00$ ), the samples undergo a structural phase transition from rhombohedral to a distorted cubic  $Pm\bar{3}m$  structure with  $a = 3.9050 \text{ \AA}$  and  $3.9088 \text{ \AA}$  respectively. The sample with  $x = 0.50$  may have a mixed rhombohedral and cubic structure. Compared to our previous studies, Ti substituted samples may increase the lattice parameters due to the slightly larger atomic radius of  $\text{Ti}^{4+}$  ( $0.605 \text{ \AA}$ ) than  $\text{Mn}^{4+}$  ( $0.530 \text{ \AA}$ ) but the whole structure still remain unchanged. [5].

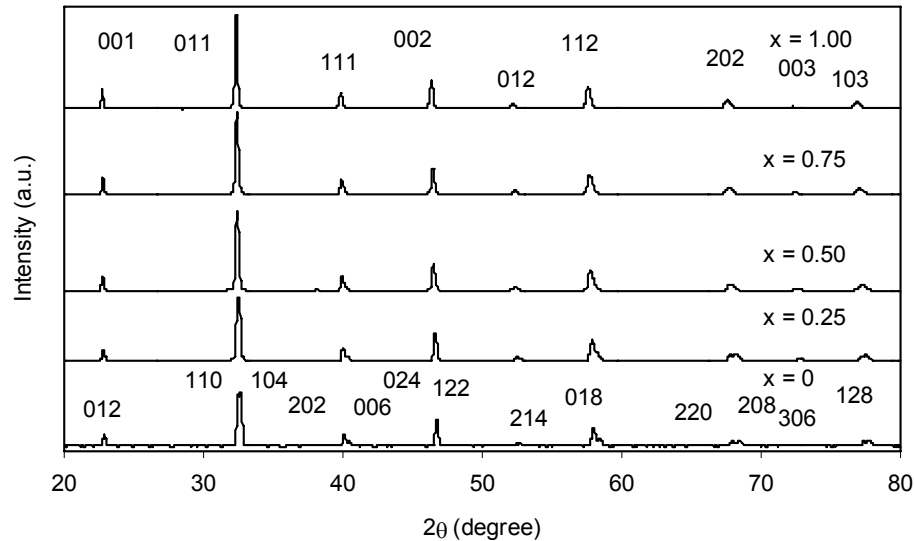


Figure 1: X-ray diffraction patterns for  $\text{La}_{0.67}(\text{Sr}_{1-x}\text{Ba}_x)_{0.33}\text{Mn}_{0.9}\text{Ti}_{0.1}$  ( $x = 0, 0.25, 0.50, 0.75$  and  $1.00$ ) samples.

Electrical resistivity of  $\text{La}_{0.67}(\text{Sr}_{1-x}\text{Ba}_x)\text{Mn}_{0.9}\text{Ti}_{0.1}\text{O}_3$  with  $x = 0.00, 0.25, 0.50, 0.75$  and  $1.00$  samples are displayed in the form of  $\ln \rho$  versus temperature,  $T$  in Figure 2. Compared to samples without Ti substitution which exhibit metal like behaviour in the whole range of temperature [5], all of these samples clearly show the metal-insulator transition temperature,  $T_P$  clearly except for  $x = 1.00$ . The resistivity for  $x = 1.00$  sample is with several orders of magnitude higher compared to others while sample with  $x = 0.25$  has the lowest resistivity. At  $T < T_P$ , the resistivity increases with temperature which is a metal-like behaviour whereas for  $T > T_P$  the resistivity decreases with temperature which is an insulator or semiconductor-like behaviour. 10 % of Ti substitution at the Mn site will replace the Mn-O-Mn bonds with the Mn-O-Ti bonds thus causing the degradation of the double exchange between  $\text{Mn}^{3+}\text{-O-Mn}^{4+}$  hence decreasing the conduction. Figure 2 also exhibits a decrement of the metal to insulator transition peak to lower temperature when Ba content is increased. This may be due to increasing columbic interactions caused by the lattice distortion. Compared to  $\text{Sr}^{2+}$ , the ionic radius of  $\text{Ba}^{2+}$  is larger than that of  $\text{La}^{3+}$ . Ba substitution with Sr lengthens the Mn-O-Mn chains. As a consequence, the lattice distortions in Ba substituted sample are larger and the energy band is narrower, thus affects the localization effects in the sample [7].  $T_P$  values of all samples are given in Table 2.

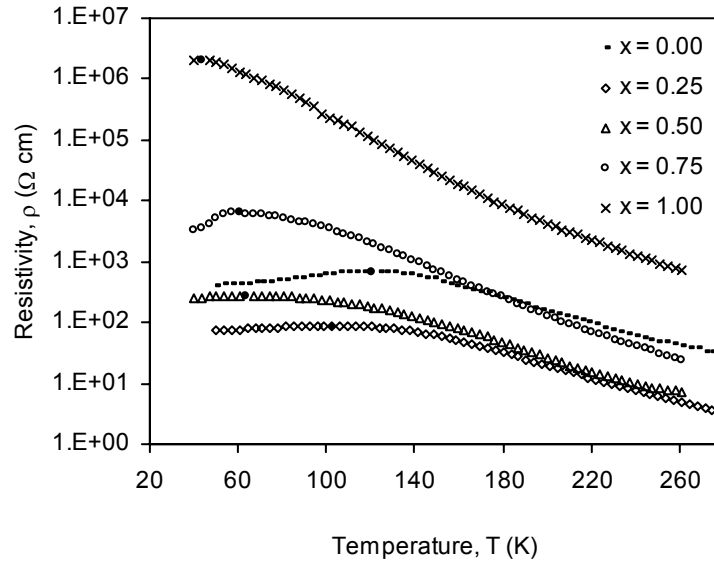


Figure 2: Resistivity ( $\rho$ ) versus temperature ( $T$ ) plots for  $\text{La}_{0.67}(\text{Sr}_{1-x}\text{Ba}_x)\text{Mn}_{0.9}\text{Ti}_{0.1}\text{O}_3$  with  $x = 0.00, 0.25, 0.50, 0.75$  and  $1.00$ .

To understand the electronic transport properties of the metal-like behaviour in the  $\text{La}_{0.67}(\text{Sr}_{1-x}\text{Ba}_x)\text{Mn}_{0.9}\text{Ti}_{0.1}\text{O}_3$  ( $x = 0.00, 0.25, 0.50, 0.75$  and  $1.00$ ) samples, the resistivity data  $T < T_P$  were fitted to an electron-electron scattering law:

$$\rho = \rho_0 + \rho_2 T^2 \quad (1)$$

and one magnon scattering law:

$$\rho = \rho_0 + \rho_{2.5} T^{2.5} \quad (2)$$

where  $\rho_0$  is the residual resistivity due to defects, domains, grain boundaries and other temperature independent scattering process,  $\rho_2$  is the resistivity of electron-electron scattering process and  $\rho_{2.5}$  is the resistivity of electron-magnon scattering process. Figure 3 shows resistivity ( $\rho$ ) versus temperature plot fitted with both equations for  $\text{La}_{0.67}(\text{Sr}_{1-x}\text{Ba}_x)\text{Mn}_{0.9}\text{Ti}_{0.1}\text{O}_3$  for the selected samples with  $x = 0.00, 0.25$ . Table 1 shows the best fitting parameters of  $\rho_0$ ,  $\rho^2$  and  $\rho_{2.5}$  with their square of the linear correlation coefficient ( $R^2$ ). However there is not enough data at low temperature for  $x = 1.00$  thus it is unable to be fitted. By comparing the  $R^2$  values we find that the resistivity data for all samples are best fitted to equation (1) which has a higher  $R^2$  value, showing that the metal-like behaviour resistivity for this compound is contributed by the electron-electron scattering process. The  $\rho_0$  give a significant contribution and plays an important role in the resistivity since polycrystalline materials contain grain boundaries.

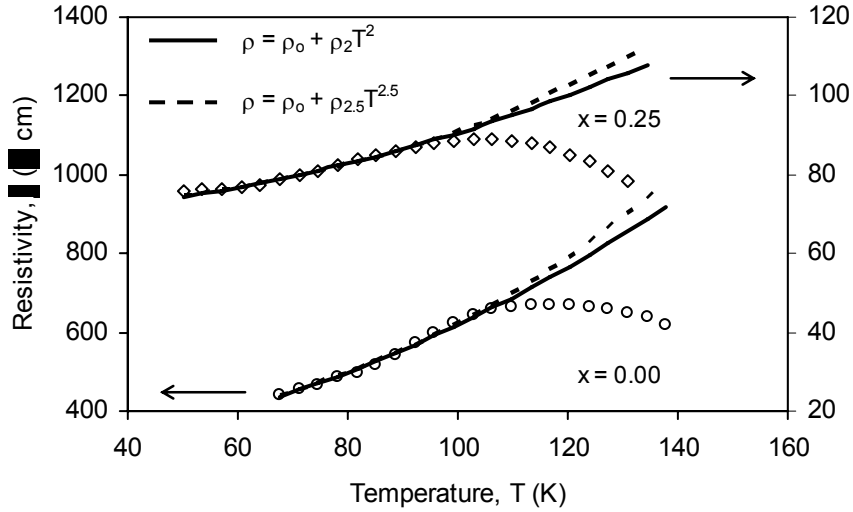


Figure 3: Fits of resistivity ( $\rho$ ) versus temperature (T) to electron-electron scattering law (solid lines) and electron-magnon scattering law (dotted lines) for  $\text{La}_{0.67}(\text{Sr}_{1-x}\text{Ba}_x)\text{Mn}_{0.9}\text{Ti}_{0.1}\text{O}_3$  ( $x = 0.00, 0.25$ ) samples.

Table 1: Values of the best fitted parameters  $\rho_0$ ,  $\rho_2$  and  $\rho_{2.5}$  for both equations with the  $R^2$  values for  $\text{La}_{0.67}(\text{Sr}_{1-x}\text{Ba}_x)\text{Mn}_{0.9}\text{Ti}_{0.1}\text{O}_3$  samples.

x	$\rho = \rho_0 + \rho_2 T^2$			$\rho = \rho_0 + \rho_{2.5} T^{2.5}$		
	$\rho_0$	$\rho_2$	x	$\rho_0$	$\rho_2$	x
0.00	285.5	0.0333	0.9891	332.5	0.0029	0.9824
0.25	69.0	0.0022	0.9968	71.3	0.0002	0.9942
0.50	229.6	0.0152	0.9895	235.8	0.0018	0.9860
0.75	1426.7	1.9964	0.9792	2061.3	0.2483	0.9750

The resistivity data just above  $T_P$  ( $T_P < T < \theta_D/2$ ) was fitted with the Mott's variable range hopping (VRH) for three dimensional system that is given by

$$\rho = \rho_0 \exp [(T_0/T)^{1/4}] \quad (3)$$

where  $T_0 = 16\alpha^3/k_B N(E_F)$ ; and  $N(E_F)$  is the density of states at Fermi level which can be calculated from the slope of  $\ln \rho$  versus  $T^{-1/4}$  plot as shown in Figure 4(a).  $\alpha = 2.22 \text{ nm}^{-1}$  is the inverse of the localization length of the trapped charge carriers [8].  $\theta_D/2$  can be estimated from the deviation from linearity of the slope in the high temperature region, where  $\theta_D$  is the characteristic Debye temperature [9]. All the estimated parameters obtained,  $T_P$ ,  $\theta_D$ ,  $T_0$  and  $N(E_F)$ , are tabulated in Table 2, and are found to be in agreement with those reported in the literature for other manganite materials [2,10,11]. According to Padmavathi et al. [10] higher  $T_0$  values indicate an increase in bending of the Mn–O–Mn bond which in turn reflects the enhancement of carrier effective mass or

the narrowing of the bandwidth, resulting in a drastic change in the resistivity and sharpening the resistivity peak in the vicinity of  $T_P$ . The  $N(E_F)$  values of the order  $10^{20}$   $\text{eV}^{-1} \text{cm}^{-3}$  are higher than the usual oxide semiconductors value of  $10^{17}$  to  $10^{19}$   $\text{eV}^{-1} \text{cm}^{-3}$  indicating an adiabatic hopping conduction [11].

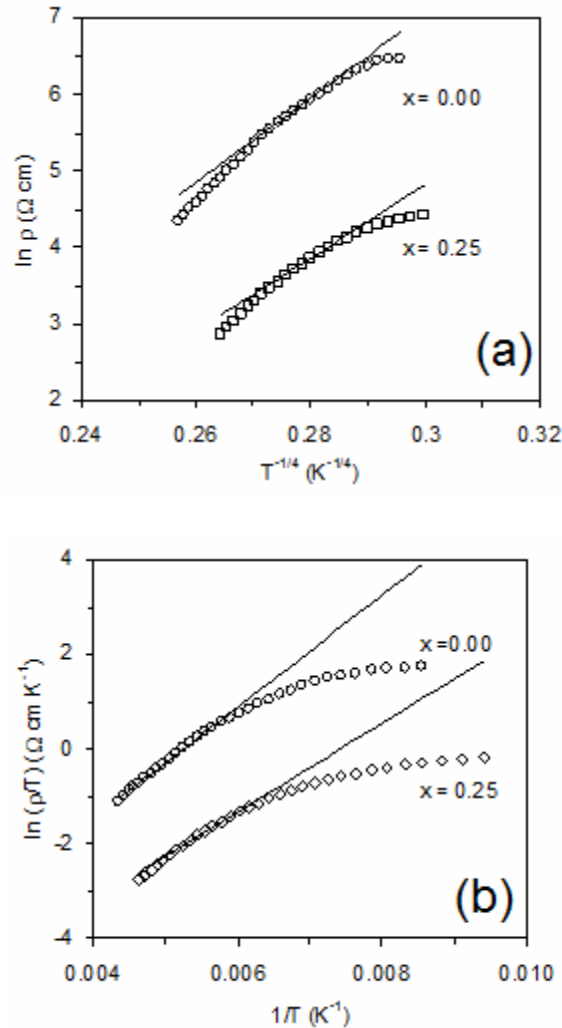


**Figure 4.** Temperature dependence of resistivity according to the (a) variable range hopping (VRH) model at  $T_P < T < \theta_D/2$  and (b) small polaron hopping (SPH) model at  $T > \theta_D/2$  for  $\text{La}_{0.67}(\text{Sr}_{1-x}\text{Ba}_x)\text{Mn}_{0.9}\text{Ti}_{0.1}\text{O}_3$  ( $x = 0.00, 0.25$ ) samples.

The small polaron hopping (SPH) model is used to fit the data beyond  $\theta_D/2$  and is given by

$$\rho = \rho_0 T \exp(E_a/kT) \quad (4)$$

where  $\rho_o$  is a pre-factor and  $E_a$  is the polaron activation energy.  $E_a$  is determined from the gradient of  $\ln \rho/T$  versus  $1/T$  graph in Figure 4(b) and shown in Table 2.  $E_a$  is found to vary with composition  $x$  and shows a minimum value at  $x = 0.25$ . A polaron is suppose to be trapped inside a local energy well of height  $E_a$  and at a certain applied temperature the polaron may hop hence inducing the electrical conduction.

**Table 2.** Metal-insulator transition temperature ( $T_P$ ), Debye temperature ( $\theta_D$ ),  $T_0$ , density of states at Fermi level ( $N(E_F)$ ) and polaron activation energy ( $E_a$ ) values for  $\text{La}_{0.67}(\text{Sr}_{1-x}\text{Ba}_x)\text{Mn}_{0.9}\text{Ti}_{0.1}\text{O}_3$  samples.

$x$	$T_P$ (K)	$\theta_D$ (K)	$T_0$ ( $\times 10^7$ K)	$N(E_f)$ ( $\times 10^{20}$ eV <sup>-1</sup> cm <sup>-3</sup> )	$E_a$ (eV)
0.00	117	346	0.92	2.21	95.53
0.25	103	326	0.51	3.97	80.51
0.50	64	304	0.60	3.37	85.11
0.75	60	278	1.96	1.04	98.25
1.00	43	264	3.68	0.55	117.56

## CONCLUSION

Structural and electrical transport properties of  $\text{La}_{0.67}(\text{Sr}_{1-x}\text{Ba}_x)_{0.33}\text{Mn}_{0.9}\text{Ti}_{0.1}\text{O}_3$  ( $0 \leq x \leq 1.00$ ) samples have been studied. The samples change from  $R\text{-}3C$  rhombohedral to  $Pm\bar{3}m$  cubic structure when Ba concentration is increased.  $\text{Ti}^{4+}$  substitution do not affect the overall structure because of its size is only slightly different from  $\text{Mn}^{4+}$ . However, Ti will replace the Mn-O-Mn bond with Mn-O-Ti bonds and greatly increases the resistivity and reduce the  $T_P$ .  $T_P$  reduces from 117 K to 60 K with increasing Ba content up to  $x = 0.75$  due to the larger size of Ba than Sr which will lengthen the Mn-O-Mn bond thus affecting the energy band. At low temperature region ( $T < T_P$ ) conduction is contributed by the domain or grain boundary mechanisms and the electron-electron scattering mechanism, which can be represented by the  $\rho = \rho_o + \rho_2 T^2$  equation. At higher temperature the conduction mechanism are connected to the variable range hopping at  $T_P < T < \theta_D/2$  and small polaron hopping  $T < \theta_D/2$  behaviour. The density of states at Fermi level ( $N(E_F)$ ) and polaron activation energy ( $E_a$ ) vary with Ba concentration. Sample with  $x = 0.25$  has the lowest resistivity and  $E_a$  values.

## ACKNOWLEDGMENT

The authors gratefully acknowledged the Department of Physics UPM for providing the research facilities and The Ministry of Science, Technology and Innovation of Malaysia for the grant under Science Fund vote: 03-01-04-SF 0009. The main author would like to thank Universiti Kebangsaan Malaysia (UKM) and The Ministry of Higher Education Malaysia for the study leave and financial support.

## REFERENCES

- [1]. Jin , S., Tiefel, T.H., McCormack, M., Fastnacht, R.A., Ramesh, R. and Chen, J.H. (1994). Thousandfold change in resistivity in magnetoresistive La-Ca-Mn-O films, *Science*, **264**: 413
- [2]. Venkataiah, G. & Reddy, P.V. (2005). Electrical behavior of sol-gel prepared  $\text{Nd}_{0.67}\text{Sr}_{0.33}\text{MnO}_3$  manganite system, *Journal of Magnetism and Magnetic Materials*, **285**: 343-352.
- [3]. Zener, C. (1951). Interaction between d-shells in the transition metals. II. Ferromagnetic compounds of manganese with perovskite structure. *Physical Review*. **82**: 403-405.
- [4]. Millis, A.J., Littlewood, P.B. and Shraiman, B.I. (1995). Double exchange alone does not explain the resistivity of  $\text{La}_{1-x}\text{Sr}_x\text{MnO}_3$ . *Physical Review Letters*. **74**: 5144-5147.
- [5]. Zalita, Z., Halim, S. A., Lim, K. P., Lee, O. J., Walter, C. P., Talib, Z. A. and Hishamuddin, Z. (2008). Structure, Magnetoresistance and Magnetism of  $\text{La}_{0.67}(\text{Sr}_{1-x}\text{Ba}_x)_{0.33}\text{MnO}_3$  Perovskite, AIP Conf. Proc., **1017**: 259-263.
- [6]. De Hoff, R.T. (1993). Thermodynamics in Materials Science, McGraw-Hill, 326.
- [7]. Mostovshchikova, E.V., Loshkareva, N.N., Bebenina, N.G. & Mukovskii, Ya.M.(2006) Optical properties of  $\text{La}_{0.85}(\text{Sr},\text{Ba})_{0.15}\text{MnO}_3$  single crystals in infrared spectral range, *Journal of Magnetism and Magnetic Materials*, **300**: e144–e146.
- [8]. Viret, M., Ranno, L. and Coey J. M. D. (1997). Magnetic localization in mixed-valence manganites. *Physical Review B*, **55**: 8067-8070.
- [9]. Mott, N.F. & Davis, E.A. (1971). Electronics Processes in Noncrystalline Materials, Oxford: Clarendon.
- [10]. Padmavathi, K., Venkataiah, G. & Venugopal Reddy, P. (2007) Electrical behavior of some rare-earth-doped  $\text{Nd}_{0.33}\text{Ln}_{0.34}\text{Sr}_{0.33}\text{MnO}_3$  manganites. *Journal of Magnetism and Magnetic Materials*, **309**: 237–243
- [11]. Banerjee, A., Pal, S., Rozenberg, E. & Chaudhuri, B.K. (2001). Adiabatic and non-adiabatic small polaron hopping conduction in  $\text{La}_{1-x}\text{Pb}_x\text{MnO}_{3+\delta}$  ( $0.0 \leq x \leq 0.5$ )-type oxides above the metal-semiconductor transition, *Journal of Physics: Condensed Matter*, **13**: 9489-9504.